

# Local mechanical properties in twisted double bilayer graphene

Alessandra Canetta,<sup>†</sup> Jean Spièce,<sup>†</sup> Sergio Gonzales-Munos,<sup>‡</sup> Khushboo Agarwal,<sup>‡</sup>  
Pauline de Crombrughe,<sup>†</sup> Viet-Hung Nguyen,<sup>¶</sup> Yuanzhuo Hong,<sup>§</sup> Sambit  
Mohapatra,<sup>§</sup> Kenji Watanabe,<sup>||</sup> Takashi Taniguchi,<sup>||</sup> Bernard Nysten,<sup>†</sup> Benoît  
Hackens,<sup>†</sup> Rebeca Ribeiro-Palau,<sup>§</sup> Jean-Christophe Charlier,<sup>¶</sup> Oleg Kolosov,<sup>\*,‡</sup> and  
Pascal Gehring<sup>\*,†</sup>

<sup>†</sup>*IMCN/NAPS, Université Catholique de Louvain (UCLouvain), 1348 Louvain-la-Neuve, Belgium*

<sup>‡</sup>*Physics Department, Lancaster University, Lancaster, UK*

<sup>¶</sup>*IMCN/MODL, Université Catholique de Louvain (UCLouvain), 1348 Louvain-la-Neuve, Belgium*

<sup>§</sup>*Centre de Nanosciences et de Nanotechnologies (C2N), CNRS, Université Paris Sud, Université  
Paris-Saclay, Palaiseau, France*

<sup>||</sup>*National Institute for Materials Science, 1-1 Namiki, Tsukuba 305-0044, Japan*

E-mail: o.kolosov@lancaster.ac.uk; pascal.gehring@uclouvain.be

## Abstract

By minimally twisting two layers of a van der Waals material, it is possible to induce atomic reconstruction in the resulting crystal, which leads to a dramatic modification of the lattice symmetry and the generation of relaxation-induced strain gradients. This has important consequences on the mechanical and electromechanical properties of the system. Here, we investigate locally those properties in minimally rotated twisted double bilayer graphene. To this end, we employ three force microscope techniques, Piezoresponse Force Microscopy, Ultrasonic Force Microscopy and Electric Heterodyne

Force Microscopy. We demonstrate that these methods are reliable and effective to visualise the Moiré pattern, to evidence the presence of non-uniform strain, and to extract the local Young's modulus in such systems. Additionally, we investigate the appearance of double domain walls, a peculiar feature of the Moiré pattern induced by strain gradients. Our results represent a further step in understanding the mechanical behaviour of twisted structures and unlock the possibility to use ~~controlled~~ strain gradients to ~~alter~~ the Moiré pattern.

## Introduction

The last few years have seen a still-ongoing interest growth in two-dimensional (2D) materials. The atomic layers in such materials are held together by weak van der Waals interactions which allow to easily cleave them and to stack different 2D atomic layers on top of each other<sup>1</sup> to create new artificial systems with completely different physical properties.<sup>2-4</sup> What is more, by twisting stacked layers with respect to each other the periodicity of the lattice of the new compound is affected, generating a so-called Moiré pattern.<sup>5</sup> Thus, the twist angle is a relevant parameter which allows to fine-tune the band structure<sup>6</sup> and lattice symmetry of the novel structures:<sup>7,8</sup> When the angle is small,<sup>9</sup> the lattice mismatch gives rise to an atomic reconstruction that ~~advantages~~ the energetically favourable stacking configurations, provoking the appearance of discrete stacking domains and domain walls.<sup>10</sup> In the large playground of twisted 2D materials, twisted double bilayer graphene (TDBG) has been proved to be an extremely versatile system, showing, at small angles, the appearance of spin-polarized correlated phase, Chern insulator at integer fillings emerging in a magnetic field, and spontaneous symmetry breaking phase transition.<sup>11-17</sup> Unlike twisted bilayer graphene, TDBG does not own a two-fold rotational symmetry.<sup>18</sup> Such broken  $C_2$  symmetry in TDBG generates the gap between the conduction and the valence band at the Dirac points of its band structure.<sup>19</sup> The separation between flat bands can be controlled by applying an external vertical displacement field, which acts on the interlayer potential.<sup>11,16,20</sup> This leads not only to an

enlarged range of twist magic angles, but also to the possibility to make the appearance of the emergent correlated electronic phases accessible and tunable by an external modulation parameter.<sup>21</sup> Beside its relevant influence on the electronic transport, the twist angle is predicted to have drastic impact on the local mechanical properties of twisted 2D systems.<sup>22-24</sup> Indeed, theoretical studies showed that, at small twist angles, atomic reconstruction occurs, causing symmetry-breaking, which introduces intralayer strain and frustrates flat band formation.<sup>25,26</sup> Such induced strain may also generate unusual features in the Moiré pattern. An example that will be investigated in this work is given by double domain walls, consisting in two single domain walls - separating different stacking domains, namely ABAB and ABCA - brought together into a unique area separating two neighbouring ABAB stacks.<sup>27</sup> Double domain walls are energetically favoured as the strain increases. Therefore, by applying a small twist angle, close to zero, it is possible to generate sufficient strain to promote the formation of double domain walls.<sup>27</sup> However, only very little experimental studies have focused on this phenomenon to date. Here, we investigate the local mechanical properties of minimally rotated ~~twisted double bilayer graphene (TDBG)~~ by means of different atomic force microscope techniques, Piezoresponse Force Microscopy (PFM),<sup>28</sup> Ultrasonic Force Microscopy (UFM)<sup>29,30</sup> and Electric Heterodyne Force Microscopy (E-HFM).<sup>31,32</sup> This allows us to image the Moiré pattern of the 2D system and to find evidence of non-uniform strain. In particular, we focus on two specific phenomena already reported in literature but that still require further study: The flexoelectric effect in the incommensurate domains and the generation of double domain walls. Moreover, we evaluate the elastic and electromechanical properties of areas with different stacking order and retrieve quantitative information about their strain dynamics and their local Young's modulus. Our results are finally compared to force-field relaxation models which enable to compute the structural morphology of the twisted pattern under uniaxial strain and Young's modulus variations across the sample.

## Results and discussion

The TDBG samples consist of two AB-stacked (or Bernal-stacked) graphene sheets rotated with respect to one another and have been fabricated by means of a dry transfer technique described in the Methods section. The two bilayers are minimally twisted with a relative angle between them close to  $\sim 0^\circ$ , in order to allow the appearance of a Moiré pattern with a large periodicity. An optical micrograph of the final structure is shown in Figure 1a.

When stacking two AB-stacked bilayers of graphene on top of each other, they can overlap with three different stacking configurations (see Figure 1b top): ABAB (Bernal stacking), ABCA (rhombohedral) and ABBC. The latter is the most unstable<sup>10</sup> as ABBC stacking of the second and third layers is energetically unfavourable. Therefore, regions characterised by the other two stacking configurations tend to expand at the expense of the ABBC stacking areas until they form large commensurate domains separated by saddle point (SP) stacking boundaries.<sup>19</sup> This leads to the formation of a Moiré pattern consisting of discrete stacking domains (see Figure 1b). In addition, a small but finite energetic imbalance between the two commensurate - Bernal and rhombohedral - stacks also exists. The latter results more stable and therefore tends to take on a convex shape due to its additional expansion.<sup>19</sup> This effect is very relevant for the formation of double domain walls, since it brings closer the single domain walls. Therefore, the intralayer strain introduced by the small twist angle results already sufficient to promote the generation of double domain walls.<sup>27</sup> To image this pattern in our TDBG samples, we employed Piezoresponse Force Microscopy, which is an established technique to study twisted materials (see Methods section). The intralayer strain gradients introduced by twisting lead to an electromechanical coupling to the out-of-plane field and enable direct visualisation of the discrete stacking domains, as already shown in previous works.<sup>33</sup> Figures 1c and d show the resulting vertical PFM amplitude (c) and phase (d) images (see Supporting Information for lateral PFM images). A set of triangular discrete stacking domains can be observed. These are defined by higher contrast interfaces, corresponding to the SP boundaries. Convex and concave domains, ABAB and

ABCA stacks, respectively, can be also distinguished.<sup>34</sup> From these images, we extracted an effective twist angle between  $0.07$  and  $0.15\sim^\circ$  using the relationship between the rotation angle  $\theta$  and Moiré wavelength  $\lambda_m$ :  $\lambda_m = (a/2) * \csc(\theta/2)$ , where  $a$  is the lattice constant of graphene.<sup>35</sup> We note that the Moiré pattern in Figure 1c consists of stretched triangular domains in contrast to the regular patterns reported previously.<sup>27,33</sup> As discussed later with the support of computational models, such stretched triangular features indicate the presence of non-uniform strain. This is induced by either atomic relaxation due to the small twist angle applied, which is extremely close to zero, or by external factors, such as wrinkles or the edge of the flakes.<sup>27</sup> In particular, an important first effect of the external strain applied is the presence of a change in orientation of the Moiré pattern, which results flipped on the bottom right corner (see Figure 1c

In the following we investigated the electromechanical and local mechanical properties of the system. To this end, we employed Electrical Heterodyne Force Microscopy (E-HFM) and Ultrasonic Force Microscopy<sup>36</sup> (UFM), respectively. Both techniques consist in a variation of the standard contact mode AFM technique and have been proven to be effective to perform electromechanical mapping with nanometer resolution. More information on these techniques can be found in the Methods section.

Figures 2b and c show the E-HFM amplitude and phase maps of the same region measured by PFM, respectively. E-HFM can be seen as an advanced version of PFM, in which the advantages offered by high-frequency excitation, as already seen in UFM,<sup>36</sup> are combined with the heterodyne conversion.<sup>32</sup> These additional features allow E-HFM to provide reliable electromechanical maps, overcoming the technical limitations of standard PFM, mostly due to electrostatic interactions, and performing the measurements at much higher frequency. Analogously to the PFM measurements (see Figure 1c), the E-HFM maps (Figure 2b-c) show an irregular Moiré pattern that consists of stretched triangles. The contrast observed along the domain walls in response to the applied electric field in Figure 2b can be attributed to the flexoelectric component of the polarisation: Strain gradients induced by atomic relaxation

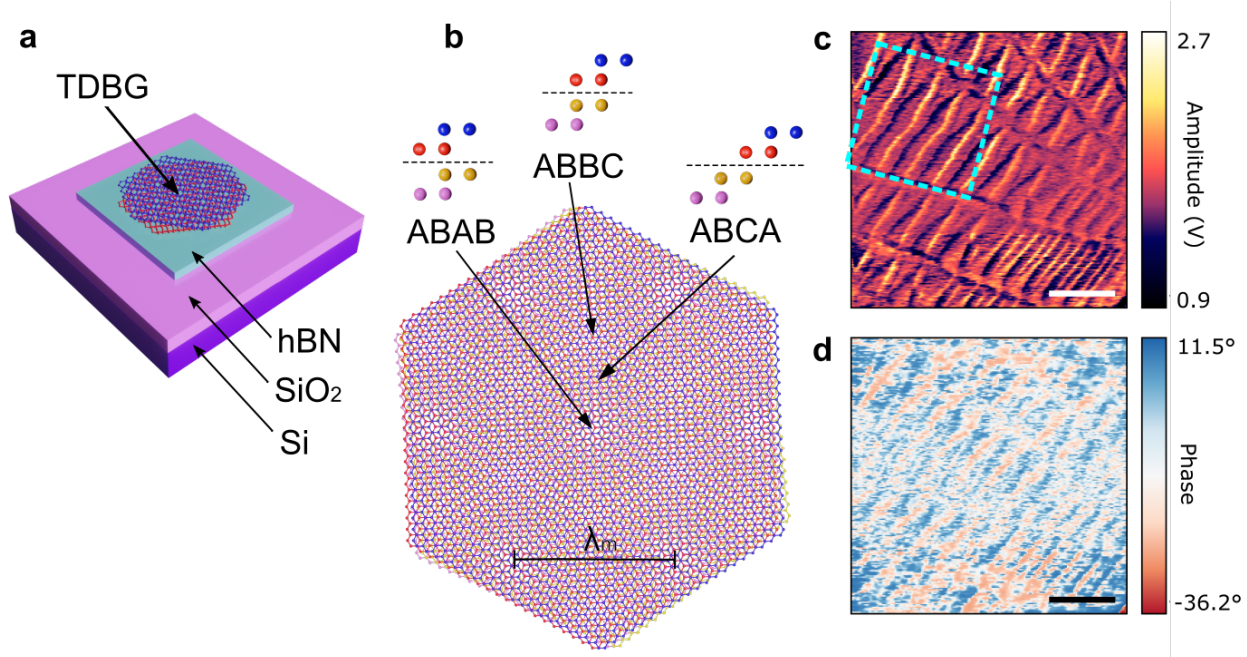


**Fig. 1. Stacking order domains in twisted double bilayer graphene and imaging of the relative Moiré superlattice by PFM.** a) Schematic of the device, consisting in two AB-stacked bilayer graphene flakes (TDBG) overlapped with a twist angle, on top of a hexagonal boron nitride (hBN) flake on a Si/SiO<sub>2</sub> substrate. b) Side views of the main stacking configurations - ABAB, ABBC and ABCA respectively - in a TDBG Moiré superlattice rotated by an angle  $\theta$  and their relative locations. The wavelength  $\lambda_m$  of the Moiré superlattice is defined as  $(a/2) * \csc(\theta/2)$ , where  $a$  is the lattice constant of graphene. c-d) Vertical PFM images (amplitude and phase, respectively) of TDBG device. The maps show evidence of the Moiré superlattice, in which different stacking domains can be distinguished, defined by the net contrast along the domain walls. The squared region delimited by the blue dashed line refers to the area where UFM measurements have been performed. Scalebars: 200 nm.

are indeed responsible for the generation of such polarisation.<sup>19,33</sup> Unlike piezoelectricity, flexoelectricity applies also to centro-symmetric structures. Therefore, the contrast retrieved in centro-symmetric ABAB and ABCA discrete domains (see Figure 2b) is due to non-uniform strain, which presence has already been confirmed in PFM measurements. Most importantly is that the two stacking domains unexpectedly show different contrast. This could be due to the energetic unbalance between ABAB and ABCA stacks, which lead to different polarization dynamics in the two regions. Thanks to the higher signal-to-noise

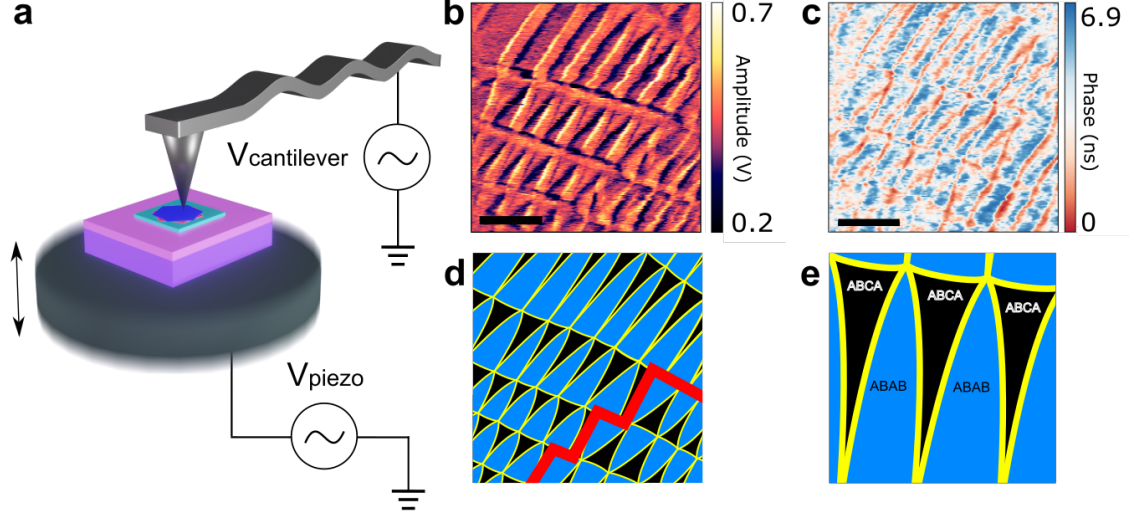
ratio of E-HFM, other subtle features can be spotted in the amplitude map: In particular, it is possible to identify the boundaries of concave (ABCA) triangular domains, which result smaller than the neighbouring ABAB domains. In order to better visualize these features, a schematic reproduction of the scanned pattern is reported in Figure 2d. ABAB and ABCA stacks, represented as blue and black regions respectively, are separated by domain walls, defined as yellow lines. Being the ABCA region smaller than the elongated ABAB stack, the two domain walls surrounding the ABCA domain result to merge beneath it and then prosecute as a unique domain wall separating the two consecutive ABAB stacks, as highlighted in Figure 2e. This specific region is defined as double domain wall (DDW).

Figure 2c shows the E-HFM phase map, from which important information related to the polarisation dynamics can be retrieved. It must be underlined that the E-HFM phase is not analogous to the standard PFM phase signal. Indeed, in the heterodyne measurement scheme, the phase relates to the delay between both actuation signals, namely  $V_{cantilever}$  and  $V_{piezo}$ . Therefore, this explains why we do not observe a contrast variation between the domain walls like reported in previous works.<sup>19</sup> Importantly, the contrast observed on the E-HFM phase map indicates the presence of different polarisation dynamics between the commensurate and incommensurate domains. This is supported by the UFM measurements that indicates that SP domains are softer. We can estimate that the phase difference lies between 0 and 6.9 ns.

In the following we use UFM to quantify the local mechanical properties of TDBG. UFM images of the region depicted in Figure 1c (see dashed blue square) are shown in Figure 2b. To quantify the local mechanical properties, we calibrated the UFM with a differential approach by comparing the UFM signals on materials with known Young's modulus: Silicon oxide, boron nitride and graphene (see Supplementary Information). This allowed us to convert the changes in UFM signal to changes in the Young's modulus.

In the UFM map (Figure 2b) domain walls, which correspond to the SP stacking, are observed as dark lines. No change in contrast is observed between neighboring ABAB and





**Fig. 2. UFM and E-HFM method and visualisation of Moiré superlattices in TDBG.** a) Schematic of the setup used for UFM and E-HFM.  $V_{cantilever}=0$  in UFM and  $V_{cantilever} = A_t \sin(\omega_t t)$  in E-HFM, while  $V_{piezo} = A_s \sin(\omega_s t + \phi)$ , with both  $\omega_s$  and  $\omega_t$  belonging in the MHz range. The arrow shows the direction of the piezotransducer vibration. b-c) E-HFM mapping (amplitude and phase, respectively) of the TDBG Moiré superlattice. d) Schematic of the stacking domain distribution of the pattern shown in (a). ABAB stacks are represented in blue, ABCA in black, separated by the yellow lines which correspond to the domain walls. The red line separate the two areas of the pattern characterized by opposite orientation. e) Close-up of the domain stacks: Each pair of single domain walls separating ABAB and ABCA regions merge into a double domain wall at the bottom, due to the elongation of the commensurate stacks. Scalebars: 200 nm.

ABCA domains. We attribute the parallel lines in the lower half of Figure 3 to double domain walls. Each of these then bifurcates into two single domain walls with a lower UFM signal strength that almost fades out at the apex of each stacking domain. The bifurcation point corresponds to the beginning of the ABCA domain (see Figure 2e). The measured width of the double domain walls is 12 nm, evaluated at full width at half maximum (FWHM). Using the calibration of the UFM we find a softening of the domain walls by 5.7 GPa  $\pm$  error (see linecut normal to the domain walls in Figure 2c). We attribute this softening to the fact that the domain walls are an energetically unfavourable region - unlike the surrounding discrete stacking domains - where atoms are held in place less strongly and a smaller force is required to displace them. This statement is in good agreement with previous works on domain walls in ferroelastic and ferroelectric materials, which show a reduction of the saddle point energy



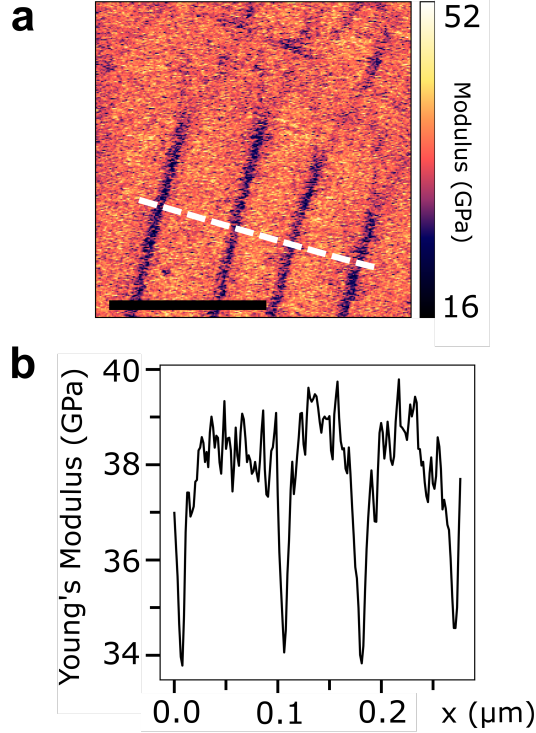


**Fig. 3. UFM visualization of Moiré pattern in TDBG.** a) UFM mapping of the TDBG Moiré superlattice. In white, a linecut perpendicular to the double domain walls is defined. c) Profile of the Young's modulus for the previously defined linecut. Scalebars: 200 nm.

in the domain wall, indicating that this is elastically softer.<sup>37,38</sup> The average UFM signal along the double domain walls results equal to  $0.147 \text{ V} \pm 0.003 \text{ V}$ , while the signal along the single domain walls - which correspond to the bifurcating lines - is  $0.203 \text{ V} \pm 0.003 \text{ V}$  (see Supporting Information for details). Using the UFM signal for the discrete stacking domains - which was found to be  $0.237 \text{ V} \pm 0.003 \text{ V}$  - as a reference, we can obtain the relative values for the signals along the double and single domain walls, respectively 90 mV and 34 mV. Thus, we can deduce that the softening along the double domain wall does not simply correspond to the overlapping of the two single domain walls, but it is actually stronger. UFM enables the study of surface and subsurface material properties with nanometric resolution,<sup>31</sup> however it has to be taken into account that such response is predominantly sensitive to elastic (modulus) and adhesive properties.<sup>36</sup> To rule out any adhesion effects, we also performed adhesion maps of the same region using PeakForce tapping. No variation of the adhesion

# THEORY RESULTS

**Fig. 4. Theory results.**

can be observed (see Supplementary information). To explain the local variation in Young's modulus we performed force-field relaxation simulations. Figure 4 shows...

## Conclusions

In this paper we exploited three different force microscopy techniques -PFM, UFM, and E-HFM- respectively- to image the Moiré in twisted double bilayer graphene rotated by an angle of  $\sim 0.1^\circ$  and investigate its mechanical and electromechanical properties. We observed the presence of non-uniform strain, manifesting as stretched triangular domains in the Moiré pattern, as confirmed by force-field simulations. We found evidence of strain-induced phenomena, in particular as the flexoelectric effect along the domain walls and the generation of double domain walls. Based on the performed measurements, we were also able to quantify the variation of Young's modulus along the various stacking domains, which resulted in a difference of approximately 5.7 GPa. Such value is in good agreement with our theoretical models. Our findings not only represent an additional step to understand the underlying physics of twisted 2D systems, but also introduced UFM and E-HFM as effective techniques to image Moiré patterns, analyze their local mechanical and electromechanical features and eventually evaluate quantitative values of important parameters such as Young's modulus.

# Methods

## Sample preparation

The twisted double bilayer (TDBG) stack was fabricated by the dry transfer technique with a Polycarbonate (PC) film (10% mass concentration) supported by a Polydimethylsiloxane (PDMS) bubble stamp. Two parts of a bilayer graphene, previously cut with an atomic force microscope,<sup>39</sup> were picked up successively with a relative twist angle of around  $1^\circ$ . The TDBG stack was deposited onto a hexagonal boron nitride flake (hBN) by transfer at room temperature without melting the PC film.<sup>40</sup> Such a cold transfer technique minimizes the contamination in the surface exposed TDBG stacks.

## Scanning Probe Microscopy

All scanning probe microscopy measurements were realised on a Multimode 3a. The lock-in detections were realised externally either with a Stanford Research System 830 or with a Zurich Instrument HF2LI.

## Piezo Force Microscopy

To perform PFM measurements, an AC bias is applied between the AFM tip and the sample to produce an electric field along the vertical direction.<sup>28</sup> This induces periodic piezoelectric strain on the sample that is detected by measuring the torsion or deflection of the AFM lever. Probe: Frequency:

## Ultrasonic Force Microscopy

To perform UFM measurements, the sample is mechanically bonded to a piezotransducer using a crystalline compound, phenyl salicylate, maximizing the ultrasonic contact.<sup>41</sup> The tip used is a regular contact mode silicon tip (Budget Sensors,  $k$ ,  $f_0$  ....) By applying a modulated AC bias ( $f \approx 4MHz$ ) to the piezotransducer, the sample is vibrated vertically

(see Figure 2a). Since the excitation frequency of the sample is much higher than the resonance frequency of the cantilever (typically 3–10 kHz), it is unable to follow the sample vibration. The cantilever therefore becomes inertially stiff.<sup>30</sup> For this reason, when in contact with the surface, the tip can indent into the sample even when the sample is much more rigid than the cantilever, making this technique extremely sensitive to the variations of the elastic properties of the sample.<sup>42</sup> The UFM response is obtained by modulating the amplitude of the ultrasonic vibration at 2.7 kHz, which is a frequency value lower than the first cantilever resonance and higher the feedback cut-off (around 1 kHz). Being the vibration amplitude cyclically varied by the modulation, the system oscillates between two regimes, linear and non-linear respectively, separated by the critical value of the ultrasonic amplitude at which the contact between the tip and the surface breaks. When entering the non-linear regime, a rectification effect that physically consists in the additional positive deflection described above is produced on the cantilever.<sup>43</sup>


### Electrical Heterodyne Force Microscopy

Analogously to UFM, the E-HFM setup involves a piezotransducer placed beneath the sample and used to make the latter oscillate at ultrasonic frequency  $f_s$ . In addition, the tip is also electrically excited by an AC bias at frequency  $f_t$ . The two ultrasonic frequencies  $f_s$  and  $f_t$  belong to the MHz range, but slightly differ from each other. The heterodyne conversion of the signal is performed by the non-linear tip-surface interaction, that in this case plays the role of the mixer, while the tip acts as local oscillator. The output signal of interest has a frequency equal to the difference  $f_s - f_t$  and it is used to perform the nonlinear signal detection. Throughout the conversion process, the phase bearing the information relative to the dynamic phenomena is conserved and appears in the output signal.<sup>44</sup> The tip-sample interaction force at the difference frequency  $\Delta f$  can be written as:

$$F_{ts}(z, t)_{\Delta f} = -\frac{1}{2}F''_{ts}(z_0)A_tA_s \cos(2\pi\Delta f t + \phi_s - \phi_t) \quad (1)$$

where  $z$  and  $z_0$  and the tip dependent and equilibrium tip-sample distance,  $A_t, \phi_t, A_s$  and  $\phi_s$  are the tip  $t$  and sample  $s$  vibration amplitude and phase.

## Acknowledgement

We thank .

## References

- (1) Geim, A. K.; Grigorieva, I. V. Van der Waals heterostructures. *Nature* **2013**, *499*, 419–425.
- (2) Sutter, P.; Sutter, E. Unconventional van der Waals heterostructures beyond stacking. *iScience* **2021**, *24*, 103050.
- (3) Li, C.; Zhou, P.; Zhang, D. W. Devices and applications of van der Waals heterostructures. *Journal of Semiconductors* **2017**, *38*, 031005.
- (4) Wu, X.; Chen, X.; Yang, R.; Zhan, J.; Ren, Y.; Li, K. Recent Advances on Tuning the Interlayer Coupling and Properties in van der Waals Heterostructures. *Small* **2022**, 2105877.
- (5) He, F.; Zhou, Y.; Ye, Z.; Cho, S.-H.; Jeong, J.; Meng, X.; Wang, Y. Moiré Patterns in 2D Materials: A Review. *ACS Nano* **2021**, *15*.
- (6) Ren, Y.-N.; Zhang, Y.; Liu, Y.-W.; He, L. Twistronics in graphene-based van der Waals structures. *Chinese Physics B* **2020**, *29*, 117303.
- (7) Carr, S.; Massatt, D.; Fang, S.; Cazeaux, P.; Luskin, M.; Kaxiras, E. Twistronics: Manipulating the electronic properties of two-dimensional layered structures through their twist angle. *PHYSICAL REVIEW B* **2017**, *95*.

- (8) Z., H.; S., K. Twistronics: a turning point in 2D quantum materials. *Electron. Struct.* **2021**, *3*.
- (9) Kerelsky, M. L. K. D. e. a., A. Maximized electron interactions at the magic angle in twisted bilayer graphene. *Nature* **2019**, *572*, 95–100.
- (10) Yoo, E. R. C. S. e. a., H. Atomic and electronic reconstruction at the van der Waals interface in twisted bilayer graphene. *Nature Materials* **2019**, *18*, 448–453.
- (11) Burg, G. W.; Zhu, J.; Taniguchi, T.; Watanabe, K.; MacDonald, A. H.; Tutuc, E. Correlated Insulating States in Twisted Double Bilayer Graphene. *Phys. Rev. Lett.* **2019**, *123*, 197702.
- (12) Cao, Y.; Rodan-Legrain, D.; Rubies-Bigordà, O.; Park, J.; Watanabe, K.; Taniguchi, T.; Jarillo-Herrero, P. Electric Field Tunable Correlated States and Magnetic Phase Transitions in Twisted Bilayer-Bilayer Graphene. **2019**,
- (13) Chebrolu, N. R.; Chittari, B. L.; Jung, J. Flat bands in twisted double bilayer graphene. *Phys. Rev. B* **2019**, *99*, 235417.
- (14) Choi, Y. W.; Choi, H. J. Intrinsic band gap and electrically tunable flat bands in twisted double bilayer graphene. *Phys. Rev. B* **2019**, *100*, 201402.
- (15) Haddadi, F.; Wu, Q.; Kruchkov, A. J.; Yazyev, O. V. Moiré Flat Bands in Twisted Double Bilayer Graphene. *Nano Letters* **2020**, *20*, 2410–2415.
- (16) Liu, X.; Hao, Z.; Khalaf, E.; Lee, J. Y.; Ronen, Y.; Yoo, H.; Haei Najafabadi, D.; Watanabe, K.; Taniguchi, T.; Vishwanath, A.; Kim, P. Tunable spin-polarized correlated states in twisted double bilayer graphene. *Nature* **2020**, *583*, 221–225.
- (17) Zhang, Y.-H.; Mao, D.; Cao, Y.; Jarillo-Herrero, P.; Senthil, T. Nearly flat Chern bands in moiré superlattices. *Phys. Rev. B* **2019**, *99*, 075127.

- (18) Lee, J. Y.; Khalaf, E.; Liu, S.; Liu, X.; Hao, Z.; Kim, P.; Vishwanath, A. Theory of correlated insulating behaviour and spin-triplet superconductivity in twisted double bilayer graphene. *Nature Communications* **2019**, *10*.
- (19) Li, Y.; Wang, X.; Tang, D.; Wang, X.; Watanabe, K.; Taniguchi, T.; Gamelin, D. R.; Cobden, D. H.; Yankowitz, M.; Xu, X.; Li, J. Unraveling Strain Gradient Induced Electromechanical Coupling in Twisted Double Bilayer Graphene Moiré Superlattices. *Advanced Materials* **2021**, *33*, 2105879.
- (20) Szentpéteri, B.; Rickhaus, P.; de Vries, F. K.; Márffy, A.; Fülöp, B.; Tóvári, E.; Watanabe, K.; Taniguchi, T.; Kormányos, A.; Csonka, S.; Makk, P. Tailoring the Band Structure of Twisted Double Bilayer Graphene with Pressure. *Nano Letters* **2021**, *21*, 8777–8784.
- (21) Zhu, Y. et al. Tunable multi-bands in twisted double bilayer graphene. *2D Materials* **2022**, *9*, 034001.
- (22) Zhang, J.; Zhao, J. Mechanical properties of bilayer graphene with twist and grain boundaries. *Journal of Applied Physics* **2013**, *113*, 043514.
- (23) Liu, A.; Peng, Q. A Molecular Dynamics Study of the Mechanical Properties of Twisted Bilayer Graphene. *Micromachines* **2018**, *9*.
- (24) Zheng, S.; Cao, Q.; Liu, S.; Peng, Q. Atomic Structure and Mechanical Properties of Twisted Bilayer Graphene. *Journal of Composite Materials* **2018**, *3*, 2.
- (25) Kazmierczak, N.; Winkle, M.; Ophus, C.; Bustillo, K.; Brown, H.; Carr, S.; Ciston, J.; Taniguchi, T.; Watanabe, K.; Bediako, D. Strain fields in twisted bilayer graphene. *Nat. Mater.* **2021**, *20*, 956–963.
- (26) Alden, J. S.; Tsen, A. W.; Huang, P. Y.; Hovden, R.; Brown, L.; Park, J.; Muller, D. A.;



- McEuen, P. L. Strain solitons and topological defects in bilayer graphene. *Proceedings of the National Academy of Sciences* **2013**, *110*, 11256–11260.
- (27) Halbertal, D. et al. Moiré metrology of energy landscapes in van der Waals heterostructures. *Nature Communications* **2021**, *12*.
- (28) Hong, S. Single frequency vertical piezoresponse force microscopy. *Journal of Applied Physics* **2021**, *129*, 051101.
- (29) Yamanaka, K.; Ogiso, H.; Kolosov, O. Ultrasonic force microscopy for nanometer resolution subsurface imaging. *Applied Physics Letters* **1994**, *64*, 178–180.
- (30) Dinelli, F.; Albonetti, C.; Kolosov, O. V. Ultrasonic force microscopy: Detection and imaging of ultra-thin molecular domains. *Ultramicroscopy* **2011**, *111*, 267–272.
- (31) Cuberes, M. T.; Assender, H. E.; Briggs, G. A. D.; Kolosov, O. V. Heterodyne force microscopy of PMMA/rubber nanocomposites: nanomapping of viscoelastic response at ultrasonic frequencies. *Journal of Physics D: Applied Physics* **2000**, *33*, 2347–2355.
- (32) Zeng, Q.; Wang, H.; Xiong, Z.; Huang, Q.; Lu, W.; Sun, K.; Fan, Z.; Zeng, K. Nanoscale Ferroelectric Characterization with Heterodyne Megasonic Piezoresponse Force Microscopy. *Advanced Science* **2021**, *8*, 2003993.
- (33) McGilly, L. et al. Visualization of moiré superlattices. *Nature Nanotechnology* **2020**, *15*.
- (34) Hattendorf, S.; Georgi, A.; Liebmann, M.; Morgenstern, M. Networks of ABA and ABC stacked graphene on mica observed by scanning tunneling microscopy. *Surface Science* **2013**, *610*, 53–58.
- (35) Kim, K.; DaSilva, A.; Huang, S.; Fallahazad, B.; Larentis, S.; Taniguchi, T.; Watanabe, K.; LeRoy, B. J.; MacDonald, A. H.; Tutuc, E. Tunable moiré bands and

- strong correlations in small-twist-angle bilayer graphene. *Proceedings of the National Academy of Sciences* **2017**, *114*, 3364–3369.
- (36) Yamanaka, K.; Ogiso, H.; Kolosov, O. Ultrasonic Force Microscopy for Nanometer Resolution Subsurface Imaging. *Applied Physics Letters* **1994**, *64*, 178 – 180.
- (37) Lee, W. T.; Salje, E. K. H.; Bismayer, U. Domain wall diffusion and domain wall softening. *Journal of Physics: Condensed Matter* **2003**, *15*, 1353–1366.
- (38) Stefani, C.; Ponet, L.; Shapovalov, K.; Chen, P.; Langenberg, E.; Schlom, D. G.; Artyukhin, S.; Stengel, M.; Domingo, N.; Catalan, G. Mechanical Softness of Ferroelectric 180° Domain Walls. *Phys. Rev. X* **2020**, *10*, 041001.
- (39) Li, H.; Ying, Z.; Lyu, B.; Deng, A.; Wang, L.; Taniguchi, T.; Watanabe, K.; Shi, Z. Electrode-Free Anodic Oxidation Nanolithography of Low-Dimensional Materials. *Nano Letters* **2018**, *18*.
- (40) Gadelha, A. et al. Twisted Bilayer Graphene: A Versatile Fabrication Method and the Detection of Variable Nanometric Strain Caused by Twist-Angle Disorder. **2021**,
- (41) Bosse, J. L.; Tovee, P. D.; Huey, B. D.; Kolosov, O. V. Physical mechanisms of megahertz vibrations and nonlinear detection in ultrasonic force and related microscopies. *Journal of Applied Physics* **2014**, *115*, 144304.
- (42) Kraatz, M.; Geisler, H.; Zschech, E. Quantification of Local Elastic Properties Using Ultrasonic Force Microscopy. *AIP Conference Proceedings* **2003**, *683*, 343–347.
- (43) Dinelli, F.; Biswas, S. K.; Briggs, G. A. D.; Kolosov, O. V. Measurements of stiff-material compliance on the nanoscale using ultrasonic force microscopy. *Phys. Rev. B* **2000**, *61*, 13995–14006.